Structure
Resource

# Controlled Bacterial Lysis for Electron Tomography of Native Cell Membranes

Xiaofeng Fu,[1] Benjamin A. Himes,[1] Danxia Ke,[1] William J. Rice,[2] Jiying Ning,[1] and Peijun Zhang[1,3,*]
[1]Department of Structural Biology, University of Pittsburgh School of Medicine, Pittsburgh, PA 15260, USA
[2]New York Structural Biology Center, 89 Convent Avenue, New York, NY 10027, USA
[3]Department of Mechanical Engineering and Materials Science, Swanson School of Engineering, University of Pittsburgh, Pittsburgh, PA 15260, USA
*Correspondence: pez7@pitt.edu
http://dx.doi.org/10.1016/j.str.2014.09.017

## SUMMARY

**Cryo-electron tomography (cryoET) has become a powerful tool for direct visualization of 3D structures of native biological specimens at molecular resolution, but its application is limited to thin specimens (<300 nm). Recently, vitreous sectioning and cryoFIB milling technologies were developed to physically reduce the specimen thickness; however, cryoET analysis of membrane protein complexes within native cell membranes remains a great challenge. Here, we use phage ΦX174 lysis gene E to rapidly produce native, intact, bacterial cell membranes for high resolution cryoET. We characterized E gene-induced cell lysis using FIB/SEM and cryoEM and showed that the bacteria cytoplasm was largely depleted through spot lesion, producing ghosts with the cell membranes intact. We further demonstrated the utility of E-gene-induced lysis for cryoET using the bacterial chemotaxis receptor signaling complex array. The described method should have a broad application for structural and functional studies of native, intact cell membranes and membrane protein complexes.**

## INTRODUCTION

Currently, cryo-electron tomography (cryoET) is the only method that offers 3D structures of pleomorphic objects, such as cells, organelles, and macromolecular assemblies, in a close-to-native state and at nanometer resolution. It has provided a wealth of information on the cellular ultrastructure of small bacterial cells (Kürner et al., 2005; Zhang et al., 2007; Khursigara et al., 2008; Briegel et al., 2009) and very thin peripheral regions of eukaryotic cells (Medalia et al., 2002; Koning et al., 2008; Carlson et al., 2010), where useful information can be recovered in cellular tomograms. With the advent of new generation direct electron detectors (Bammes et al., 2012; Campbell et al., 2012; Bai et al., 2013; Li et al., 2013) and phase plates (Fukuda et al., 2009; Murata et al., 2010; Barton et al., 2011; Guerrero-Ferreira and Wright, 2014), the application of cryoET to study small prokaryotic cells will potentially produce results of significant impact in the field of prokaryotic cell biology (Li and Jensen, 2009; Milne and Subramaniam, 2009). The main limitation for obtaining high quality cellular tomograms is the specimen thickness, which is typically close to 1 μm for most bacterial cells. To address this issue, methods have been developed to physically reduce the thickness of frozen-hydrated specimens, including vitreous sectioning (Zhang et al., 2004; Al-Amoudi et al., 2005) and, more recently, cryo-focused-ion-beam (cryoFIB) milling (Marko et al., 2007; Hayles et al., 2010; Wang et al., 2012). Others have used genetic approaches to create minicells (Briegel et al., 2012; Liu et al., 2012), or biochemical approaches to make leaner cells by varying the cell culture conditions (Trueba and Woldringh, 1980). While these approaches facilitate 3D visualization of intracellular structural details, cryoET analysis of cell membrane structures and important membrane protein complexes within intact, native cell membrane remains difficult.

Conventional cell membrane preparation methods, such as ultracentrifugation of bacterial cell lysates by lysozyme and EDTA treatment, usually yield heterogeneous membrane fragments (Poole, 1993). Phage lysis offers an attractive alternative approach for producing intact native cell membranes in growing cells; in this case, intact ghost cells, which have much of the cytoplasm removed, are generated. Bacterial phages use two strategies to achieve lysis of the bacterial host cells in a timely manner: double-stranded DNA (dsDNA) phages, such as lamda phage, employ a complex binary system with a holin and a muralytic enzyme, endolysin, for lysis; and small single-stranded DNA and single-stranded RNA phages, on the other hand, produce host lysis by creating a single lytic protein without muralytic activity (Young, 1992; Wang et al., 2000). A remarkable example of this is the small DNA phage ΦX174, in which a single gene, E, which encodes a 91 amino acids integral membrane protein, mediates host cell lysis at a concentration of 100–300 molecules per cell (Young and Young, 1982; Maratea et al., 1985). Furthermore, overexpression of the E gene product is sufficient to cause rapid cell lysis (Young and Young, 1982). Owing to the simplicity and unique properties of the E gene, here, we employ the E lysis system to produce intact bacterial cell membranes for high resolution cryoET structural analysis. We demonstrate that ghost membranes can be obtained via spot lesion upon E gene induction. CryoET analysis of E gene-induced cell ghosts showed highly ordered chemotaxis membrane receptor signaling complexes, with up to 25 Å resolution in a single cellular tomogram. The methods described here will be of great interest to those studying the biophysical and

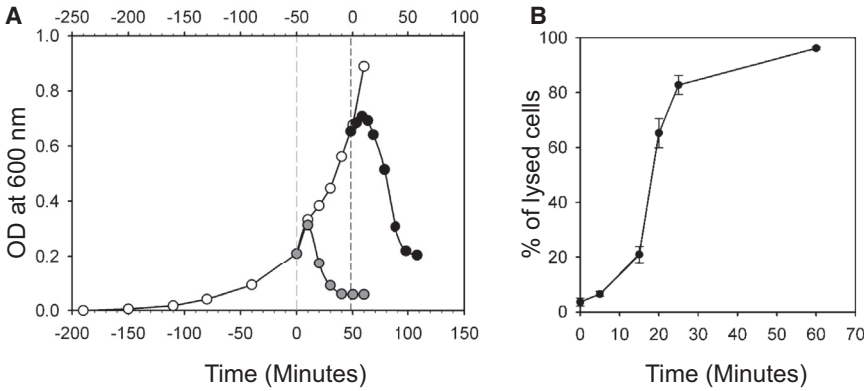


**Figure 1. Phage ΦX174 E Gene Induces Rapid Bacterial Cell Lysis**

(A) Growth and lysis curves of *E. coli* cultures carrying E gene expression plasmid. The OD at 600 nm was measured in control cells (open circles) or after induction of the E gene product at an $OD_{600}$ of 0.2 (gray, designated time 0 on the bottom axis) or 0.65 (black, designated time 0 on the top axis).

(B) The percentage of lysed cells observed in *E. coli* samples at the indicated time after E gene induction. The number of lysed cells was counted from 10 low magnification TEM images and averaged for each time point (~300 cells in each sample). The SD in each sample was plotted as the error bar.

biochemical properties of cell membranes and membrane proteins in their native environment.

## RESULTS

### Expression of ΦX174 E Gene Results in Rapid Lysis of *E. coli* Cells

Expression of phage ΦX174 gene E was previously shown to be necessary and sufficient for the lysis phenomenon exhibited by phage-infected cells (Young and Young, 1982). To examine the structural effect of E gene on host cells, we used a tightly controlled plasmid expression system to produce E gene product in *E. coli* cells. Under a tacP promoter and a lacIQ repressor (Roof et al., 1997), E gene expression was triggered by addition of isopropyl β-D-1-thiogalactopyranoside (IPTG), at two different time points, optical density (OD) = 0.2 or OD = 0.6, during the log phase of cell growth. In both cases, the OD of the cell culture started to decrease within 10 min of IPTG addition, suggesting a very rapid activation of cell lysis by E gene product (Figure 1A). The lysis process was nearly complete at about 30 min. This is consistent with previously reported results (Bernhardt et al., 2001a, 2002) and, thus, supports a model wherein E-mediated lysis occurs during cell division by inhibiting the peptidoglycan synthesis enzyme MraY (Bernhardt et al., 2000).

The efficiency of E-mediated lysis was further quantified by examining the morphology of individual bacterial cells, using a transmission electron microscope (TEM). Cultured *E. coli* cells were collected and frozen under high-pressure at the indicated time points after IPTG induction, followed by freeze-substitution, resin embedding, and sectioning. TEM imaging revealed individual cells undergoing lysis, as evidenced by their less dense cytoplasm compared to intact cells (Figures 2A–2C). To quantify the lysis process, the fraction of cells undergoing lysis was determined at several time points after IPTG induction from electron microscopy (EM) micrographs. As illustrated in Figure 1B, *E. coli* cells begin losing cytoplasm very quickly upon E gene induction, as early as 5 min postinduction. Quantitative cell morphology analysis indicates that the onset of lysis was actually earlier than that measured by OD. This is likely because the majority of cells were still growing at the early OD measurements. At 25 min, more than 80% of cells were affected, and at 60 min, near 95% of the cells had undergone lysis. Thus, compared to the complex binary endolysin/holin lysis system (Young, 1992), E-mediated bacterial lysis is remarkably simple, effective, and efficient.

### E-Mediated Lysis Produces Whole Cell Ghosts through Spot Lesion

To further characterize the structural changes during E-mediated cell lysis, cells at different lysis stages were imaged by TEM. As shown in Figure 2, before E-gene induction, all cells displayed a dense cytoplasm, and many were actively dividing (Figures 2A and 2D). At 25 min after induction, the majority of cells were either partially (arrowhead) or completely (double arrowhead) lysed, and only a small fraction of cells remained intact (arrow) (Figures 2B and 2E). After 60 min, nearly all the bacterial cells had lost cytoplasm. In contrast to other cell lysis methods, which produce only membrane fragments (Poole, 1993), E gene-mediated lysis maintained and preserved the cell membranes and cell shape (Figures 2E and 2F). More interestingly, upon close inspection of those cells captured instantly at the early lysis stage (Figures 2G and 2H), we found localized lesion spots from which cells seemed to be losing their cellular content: the cell membrane appeared to be punctured with the cytoplasm ejected through the compromised membrane. We further characterized the 3D morphology of lysed cells using ion-abrasion scanning EM. Consistent with our previous observation, a majority of *E. coli* cell ghosts remained as rod shaped membrane shells, with a few occasional spheroplasts (Figure 2I).

### Membrane Proteins and Associated Protein Complexes Are Retained

To determine whether membrane proteins and protein complexes remain associated with the cell membrane after E-mediated lysis, we examined the lysed cells for the presence of the chemotaxis membrane receptor signaling complex, which is composed of transmembrane receptors, a cytoplasmic histidine protein kinase, CheA, and a small soluble cofactor, CheW. Cell ghosts were pelleted after varying periods of E-gene induction and analyzed for the presence of membrane receptors and CheA. As shown in Figure 3A, throughout the lysis process, up to near completion (30 min), the chemotaxis membrane receptor and CheA remained associated with the ghost membranes, with little detected in the cell supernatant, even when very little

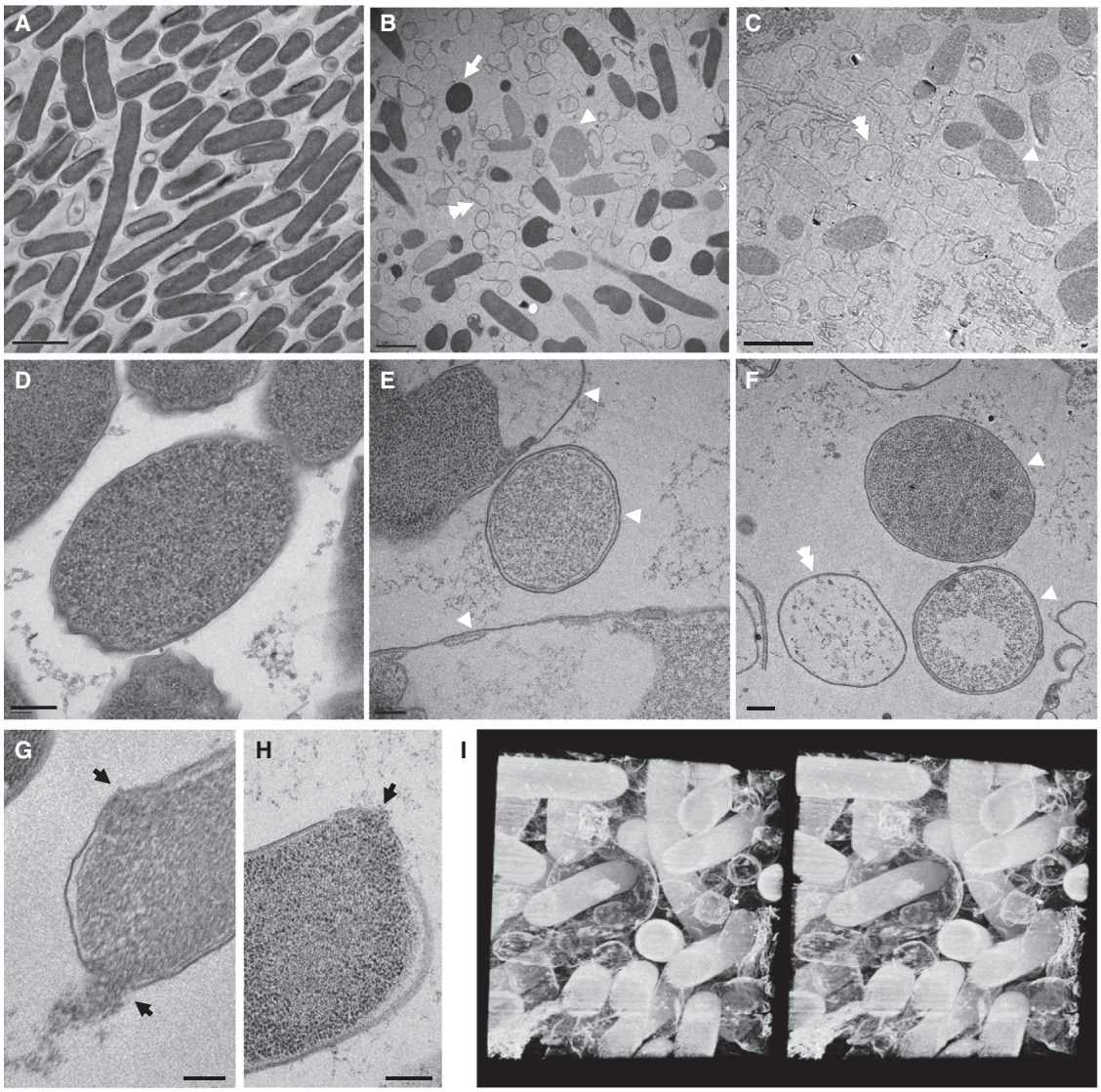


**Figure 2. Electron Microscopic Characterization of E Gene-Induced Cell Lysis**

(A–F) TEM images of thinly sectioned *E. coli* cells, recorded at low (A–C) or high (D–F) magnifications. The cells were subjected to high-pressure freezing at 0 min (A and D), 25 min (B and E), or 60 min (C and F) after IPTG induction, followed by freeze-substitution and resin embedding. White arrows, arrowheads, and double arrowheads indicate unlysed, partially lysed, and completely lysed cells, respectively.

(G and H) TEM images capture the cells in the lysis process. Black arrows indicate the lesion sites in cell membranes, resulting in the release of cytoplasm.

(I) Stereo view of a 3D volume from *E. coli* cell samples at 30 min after E gene induction.

Scale bars, 2 μm (A–C) and 200 nm (D–H).

cytoplasm was left (Figure 3B). This was also true for $F_0F_1$ ATP synthase when tested using antibodies against soluble $F_1$ epsilon subunit (Figure 3A, lower panel). Thus, the cell ghosts produced by E-lysis are good candidates for biochemical, biophysical, and structural analysis of membrane protein complexes.

## Cryo-EM and CryoET Analysis of Ghost Cell Membranes

Because E-mediated lysis produces cell ghosts with intact native membranes, such a system could have great utility for structural, biophysical, biochemical, and functional studies of membrane proteins. We thus assessed its usage for structural analysis of cell membranes and membrane-associated proteins by cryoEM and cryoET. *E. coli* cells at an early stage of E-gene expression (12 min) were directly plunge frozen from cell culture and imaged by cryoEM. Figure 4A shows the cryoEM image of a lysed cell (light density, black arrow) and an intact unlysed cell (dark density, orange arrow) captured in the same field. At an early stage such as this, about 20% of the cells have begun to undergo the lysis process, exhibiting reduced cell thicknesses (Figure 4B, red), and more cells become thinner 30 min post E-gene induction (Figure 4B, blue). This is consistent with the previously proposed model for E gene-mediated lysis, in which the E gene product acts on the bacterial cell wall by inhibiting

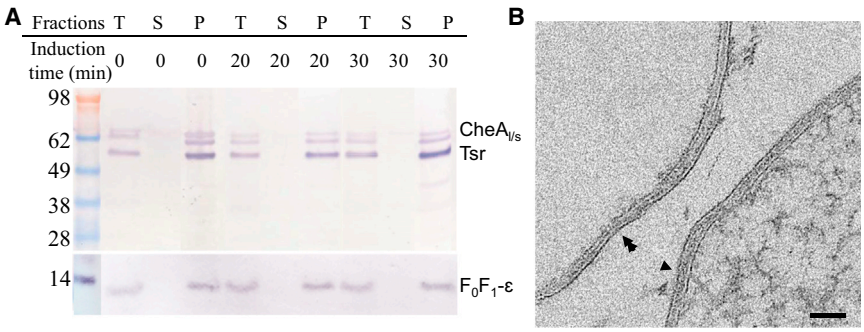


**Figure 3. Analysis of Chemotaxis Membrane Receptor Signaling Complex in E-Lysed Cells**

(A) Western blot analysis of bacterial chemoreceptors and the associated soluble histidine kinase, CheA, in total cell (T), S, and P fractions at the indicated post E gene induction time. Both chemotaxis membrane receptors (Tsr) and soluble $CheA_{l/s}$ (long and short forms), as well as the epsilon subunit of $F_0F_1$ATP synthase remain in the P fractions.

(B) A TEM projection image of a sample 30 min after E gene induction shows intact cell membranes. Arrowhead and double arrowhead indicate a partially lysed and a completely lysed cell, respectively.

Scale bar, 50 nm.

MraY, leading to cell lysis during cell division (Bernhardt et al., 2001a). In fact, the process of cells spouting their cytoplasmic content, at the onset of lysis, was evident in our cryoEM images (Figure 4). For example, in Figure 4C, a pool of ribosome molecules that was presumably just released from the bacterial cell is found surrounding the ghost cell, suggesting that these molecules were released at the moment of plunge-freezing. Such ribosomal pools were frequently observed around cell ghosts at the early stages after E gene induction. The membrane structures were well preserved, with the inner cell membrane, peptidoglycan, and outer membrane clearly seen (Figures 4C and 5B) and comparable to those observed in vitreous sections (Zhang et al., 2004) and cryoFIB milled cell lamella (Wang et al., 2012). Furthermore, the onset of lysis was instantaneously captured by rapid freezing and cryoEM (Figure 4D); the cellular content was observed to be discharging through small lesion holes, about 50 nm in size (Figure 4D, black bracket), where the inner membrane and peptidoglycan appear disintegrated. The data indicate that E-lysis occurs through small individual lesion spots where cytoplasm is ejected, leaving the major portion of the cell membrane intact.

We also carried out 3D structural analysis of E-lysed cell ghosts by cryoET. The spot lysis observation was confirmed in 3D tomograms (Figure 5A, black arrowhead; Movie S1 available online), with pore sizes of about 50–100 nm. This is a direct observation of lysis holes spanning two membranes in a native hydrated environment. Attempts to visualize the membrane lesions by conventional ultrathin-section EM have been unsuccessful, in part because of the structural deformations associated with the multiple fixation, dehydration, and staining steps (Kellenberger et al., 1992). CryoET allows chemical-free preservation of whole cells within milliseconds and provided better than 5 nm resolution. Interestingly, in the 3D tomograms, the inner and outer membranes at the lesion spot appear to be connected at the rim, sealing the periplasmic space at the pore (Figure 5A; Movie S1), reminiscent of the nuclear pore in eukaryotic cells. The cellular content moving through the pore is clearly visible in Figure 5A (dashed profile). Since the cell had just begun to leak its content, the thickness of the cell is only partially reduced to ~250 nm (Figure S1A), compared to the cells that are further along in the lysis process, at 100–150 nm thickness (Figures 5B–5D, S1B, and S1C). Presumably due to the release of pressure within lysed cells, the rod-shape ghosts collapse into two layers of cell envelopes upon plunge freezing, and the inner membrane sometimes retracts from the cell wall (Figure 5B; Movie S2), but was often kept in place in regions where flagella motors were anchored across the two membranes (Figure 5C; Movie S3). The fine structure of the peptidoglycan was clearly resolved in the lysed ghosts (Figures 5B and 5C, white arrow), similar to those seen in vitreous sections (Zhang et al., 2004). DNA strands and protein complexes released from the cell were clearly visible adjacent to the cell (Figures 5B and 5D).

Remarkably, the transmembrane chemotactic receptor signaling complexes were maintained in a highly ordered crystalline arrangement upon E-mediated lysis (Figure 5D; Movie S4), with a resolution of at least 25 Å, as seen in Fourier transform of a single receptor cluster in the tomogram (Figure 5D, top inset). The quality of the tomogram is much better than what has been previously achieved for cellular tomograms without subvolume averaging. A subtomogram averaging of ~400 trimeric chemotaxis signaling units yielded a 3D density map comprising a trimer of CheA dimer/receptor complexes (Figure 5D, bottom inset, Figure S2A), consistent with the previous subtomogram averaged structures from other bacterial species (Briegel et al., 2012; Liu et al., 2012). The data from a single native receptor cluster suggest that the chemotaxis arrays in *E. coli* cells are highly ordered, in contrast to the chemotaxis arrays observed in other cell types (Khursigara et al., 2008). While previous studies were carried out with thick specimens, such as whole cells (~0.6–1 μm thick) with limited resolution, the cell ghosts used in this study were mainly composed of two layers of cell envelope (~150 nm thick) and yielded much more detailed information at a higher resolution. Therefore, among the many different methods applied to generate samples for cryoEM and cryoET, such as engineered minicell (Briegel et al., 2012; Liu et al., 2012), vitreous sectioning (Zhang et al., 2004), or whole cell preparations (Zhang et al., 2007), the E-lysis procedure provides the highest quality native receptor clusters for 3D structural analysis.

## DISCUSSION

The mechanism of E-mediated lysis is still not fully understood, although the current model of MraY inhibition is consistent with our results (Roof et al., 1997; Bernhardt et al., 2000, 2001a; Mendel et al., 2006; Zheng et al., 2008). Further biochemical and structural studies are needed to understand the molecular mechanism of E-gene product action on cell membrane integrity and lysis (Zheng et al., 2009). Nevertheless, with millisecond

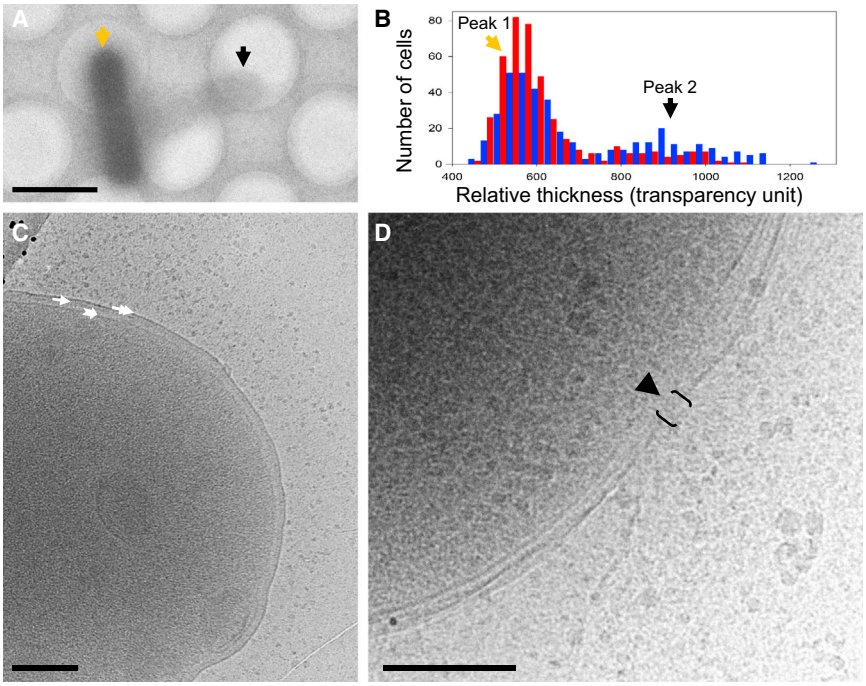


**Figure 4. CryoEM Analysis of E Gene-Induced *E. coli* Cell Lysis**

(A) A low magnification projection image of *E. coli* cells shows an unlysed cell (orange arrow) and a partially lysed cell with a higher electron transparency (black arrow).

(B) Distribution of the thickness of the cells at 15 (red) and 30 (blue) min post E-gene induction. The orange and black arrows indicate the unlysed and lysed cell populations, respectively.

(C) A high magnification view of the partially lysed *E. coli* cell shown in (A). Ribosome molecules were instantaneously released from the lysing cell at the moment of freezing, as seen by the pooling around the cell. Inner membrane, peptidoglycan, and outer membrane are indicated by chevron arrow, arrow, and double arrow, respectively.

(D) A cryoEM projection image captures an *E. coli* cell at the onset of lysis. The arrowhead points to the lesion spot where cytoplasm, containing DNA and protein molecules, is being ejected. The size of the lesion is indicated by a black bracket.

Scale bars, 2 μm (A) and 200 nm (B and C).

cryo-fixation, which allows instantaneous capturing of biological processes under native conditions, the lethal holes caused by the E gene product of bacteriophages and the resulting discharge of bacterial cytoplasm have now been directly observed in vivo by cryoEM and cryoET. Unexpectedly, the size of the membrane lesion holes caused by the E gene product is only 50–100 nm (nano-sized), much smaller than that produced by holin S105 protein, which exceeds 300 nm to μm (microsized) (Dewey et al., 2010), and smaller than the large transmembrane tunnel structures observed in lysed bacterial cells (Witte et al., 1990a, 1990b; Lubitz et al., 1999). Distinct from the holing-endolysin lysis system with λ phage (Dewey et al., 2010), the nano-sized lesion holes transverse both bacterial membranes, creating a small channel from which the cytoplasm is ejected. In addition, unlike the binary holing-endolysin lysis system (Wang et al., 2000), in which spheroplasts were produced with extensive damage of the cell wall through murein degradation by endolysin (Dewey et al., 2010), the *E. coli* cell ghosts produced by E-mediated lysis maintained the rod shape with very limited cell wall damage. Further, membrane proteins and protein complexes are retained within the ghost membranes with minimal disruption.

Several methods for bacterial cell membrane preparation have been described, including chemical and mechanical disruption or disintegration of cell wall, as well as freezing and thawing of bacterial cells (Leduc et al., 1982; Poole, 1993). Compared to these commonly used methods, such as treatment with penicillin or lysozyme-EDTA, which generally produce spheroplasts and membrane vesicles (Kaback, 1972), the advantages of membrane preparation by E-lysis are 5-fold: (1) it is a simple system, since expression of a single 91 amino acid E protein causes cell lysis at a concentration of 100–300 molecules per cell (Maratea et al., 1985); (2) it is quick, overexpression of the E gene product is sufficient to cause rapid cell lysis in less than 10 min; (3) lysed cells release cytoplasm through a nano-sized lesion, while a majority of the cell membrane remains intact; (4) both inner and outer membranes are retained (Witte and Lubitz, 1989), along with membrane proteins and associated protein complexes; and (5) E-gene lysed cells retain their rod-shape, but have lost intracellular content through focal lesion. When subject to freezing, the cell envelope collapses, yielding very thin cell ghosts with just two layers of cell envelope, compared to the round spheroplasts with a 0.5–1 μm thickness. The method we described here, using controllable E-mediated lysis to rapidly produce intact membrane envelope, provides superior signal-to-noise ratios for structural study of native cell envelope and membrane protein complexes, as demonstrated by cryoET of bacterial chemotaxis signaling arrays and $F_0F_1$ATP synthase. We anticipate that such an intact native membrane system, generated by E-mediated cell lysis, will not only constitute a useful tool for cryoEM and cryoET structural studies of membrane receptor complexes, but also for biophysical and biochemical characterization of membranes and membrane protein complexes in a native environment, as well as for protein antibiotic (Bernhardt et al., 2001b) and vaccine development against bacterial pathogens (Szostak et al., 1996, 1997).

## EXPERIMENTAL PROCEDURES

### Bacterial Strains, Plasmids, and Cell Culture

Wild-type *E. coli* K-12 strain RP437 cells (Parkinson and Houts, 1982) carrying plasmid pRY100 (a kind gift from Dr. Ry Young, Texas A&M University) (Roof et al., 1997) were grown in tryptone broth (1% tryptone and 0.4% NaCl, pH 7.0), supplemented with 100 μg/ml ampicillin. The plasmid pRY100 has the phage ΦX174 lysis E gene under a tacP promoter and a lacIQ repressor control. RP437 cells carrying pRY100 were grown to an $OD_{600}$ of 0.2 or 0.6, and E gene expression was induced by 0.5 mM IPTG. The progress of cell lysis was

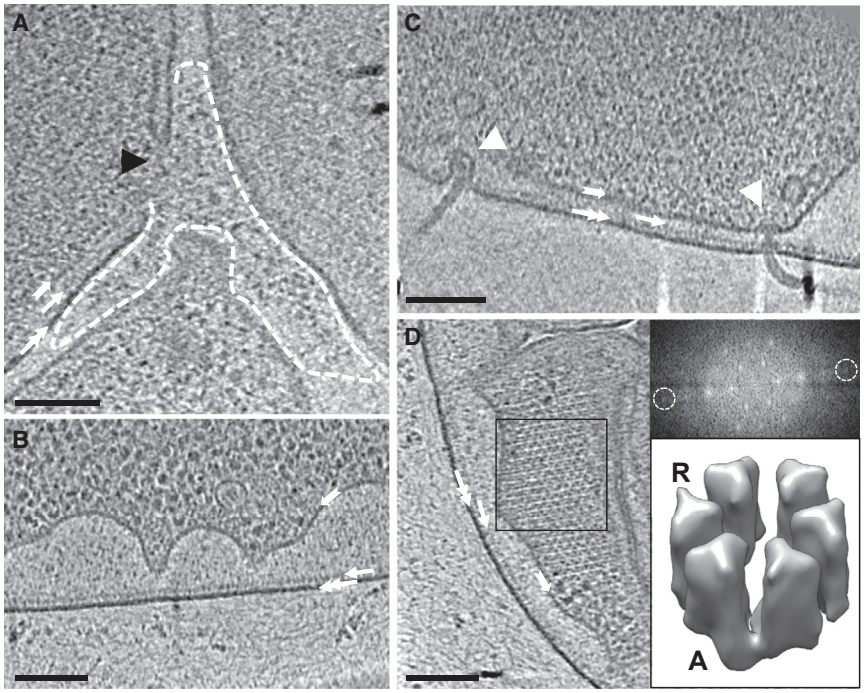


**Figure 5. CryoET Analysis of *E. coli* Cell Membranes Generated by E Gene-Induced Cell Lysis**

(A) A lysis pore (black arrowhead) across the two cell membranes is captured by rapid freezing and visualized in 3D tomographic slices. The spouting cytoplasm is indicated by dashed profile. See also Movie S1. Inner membrane, peptidoglycan and outer membrane are indicated by the chevron arrow, arrow, and double arrow, respectively, in each panel.

(B) The cytoplasmic membrane (chevron arrow) retracts from the cell wall due to release of the pressure inside the cell. DNA strands and ribosome molecules are clearly seen in the surroundings of the partially lysed cell. See also Movie S2.

(C) Flagella motors (white arrowheads) are anchored across the two membranes in a partially lysed cell. See also Movie S3.

(D) High resolution tomographic reconstruction of chemotaxis receptor signaling complexes within the cell membrane of partially lysed cell. See also Movie S4. The ordered receptor signaling array diffracts to 25 Å resolution, as indicated by the circles in the Fourier transform (upper inset) calculated from a 15 nm thick tomographic slice from the boxed area. Subtomogram averaging yielded a 3D density map of the trimeric chemotaxis signaling unit containing three CheA dimers ("A") and six receptor trimers of dimers ("R") (lower inset).

See also Figures S1 and S2. Scale bars, 100 nm.

monitored at $OD_{600}$ from the beginning of culture until 60 min after addition of IPTG. The lysis profiles were obtained by measuring $OD_{600}$ at different time points.

### Protein Analysis with Western Blot

The same volume of *E. coli* cells was withdrawn from noninduced cultures and from E gene-induced cultures at 20 or 30 min post IPTG addition. There were 6 μl samples that were mixed with 4 × lithium dodecyl sulfate (LDS) loading buffer (Invitrogen) supplemented with 10 mM dithiothreitol for SDS-PAGE analysis (T). The remaining sample was pelleted at 20,000 × *g* with an Eppendorf centrifuge 5417R for 15 min and supernatants (S) and pellets (P) were mixed with 4 × LDS loading buffer for gel analysis. Total, S, and P samples were loaded on 4%–12% SDS-PAGE. Proteins were electrophoretically blotted to nitrocellulose membranes. Chemotaxis receptors and CheA proteins were detected by probing with receptor-specific and CheA-specific polyclonal antibodies. The $F_1$ component of $F_0F_1$ ATP synthase was detected by probing with polyclonal antibodies that recognize the epsilon subunit. Bands were developed and revealed using BCIP/NBT liquid substrate system (Sigma B1911) with conjugated anti-rabbit antibodies.

### EM of High Pressure Freezing and Freeze-Substituted Samples

Bacterial cell culture samples (30 ml) were collected at 0, 5, 15, 20, 25, or 60 min after IPTG addition and were pelleted at 2,500 × *g* for 15 min in a Sorvall (RC-3C Plus) swing rotor. The cell P were put on ice and transferred to Leica EM PACT2 membrane carriers (1.5 mm × 0.2 mm) for high pressure freezing in EM PACT2 (Leica Microsystems), at an average pressure of 2,000 bars (Studer et al., 2001). The frozen cells were then transferred to a freeze-substitution machine, Leica EM AFS (Leica Microsystems), for a 5-day solvent substitution. Briefly, frozen samples were warmed from −196°C to −90°C over a 3-day period in a precooled (−90°C) 1% $OsO_4$ and 0.1% uranyl acetate mixture dissolved in acetone. Samples were then gradually warmed to room temperature over 18 hr and subsequently rinsed in acetone for further resin infiltration and embedding in Epon. Ultrathin sections (65 nm) were cut with a Reichart Ultracut and laid on 300 mesh carbon-coated EM grids. The thin sections were poststained with 2% uranyl acetate in methanol for 10 min, followed by Reynold's lead citrate for 7 min (Reynolds, 1963), and were examined with a Tecnai F20 electron microscope (FEI.) equipped with a 4,000 × 4,000 camera (Gatan). Projection images were recorded at a magnification of 2,500× and 19,000×.

### FIB/Scanning Electron Microscope

Resin blocks were attached to scanning electron microscope (SEM) stubs using double sided carbon sticky tape, then painted with colloidal silver (EMS). The blocks were made conductive by coating with Au/Pd in a Denton sputter coater (25 mA current for 5 min at 50–60 milliTorr) then inserted into a FEI Helios NanoLab 650 (FEI) for FIB milling. Areas were identified by viewing with the e-beam at 20 kiloelectrovolt (keV) then coated with 1 um thick platinum for protection. A trench was dug in front of the area to be milled, and side trenches were dug adjacent to this area. The FEI Slice and View software (made and sold by FEI Company and installed on FEI Helios Nanolab 650) was used to collect slices using a slice width of 20 nm and a horizontal field width of 10 μm (4.88 nm/pixel). Sections were imaged at a −38 degree viewing angle at an e-beam voltage of 2 keV and 100 picoamperes current. Following collection, images were aligned using IMOD software (Kremer et al., 1996).

### CryoEM and CryoET

There were 3–5 μl of uninduced and E-gene induced (12 min) *E. coli* cell samples, at an $OD_{600}$ of 0.5, that were withdrawn directly from cultures and placed on R2/1 Quantifoil grids (Quantifoil Micro Tools). There were 2 μl of 15 nm gold beads that were applied to the EM grids to serve as fiducial markers for tomographic alignment. The grids were manually blotted and plunge-frozen in liquid ethane maintained at approximately −180°C using a homemade manual plunger. For projection images, grids containing plunge-frozen cells were loaded onto a Gatan model 626 cryo-holder maintained at temperatures below −180°C and imaged using a Tecnai F20 transmission electron microscope equipped with a field emission gun (FEI) and a Gatan 4,000 × 4,000 CCD camera (Gatan). Low dose (20 electrons per angstrom square) projection images were recorded at a magnification of 31,000× with under focus values ranging from 2 to 5 μm.

For 3D cryoET, frozen-hydrated EM grids were placed in cartridges and loaded into the cryo-transfer system of a Polara G3 microscope (FEI). The Polara microscope was equipped with a field emission gun operating at 300 keV.

A series of low dose projection images of *E. coli* cells were recorded at a tilt angle range from 70° to 70°, at a nominal magnification of 27,500×, with under focus values between 5–8 μm. The total dose used for each tilt series was typically ~60–80 $e^-/Å^2$. Tilt series were aligned using 15 nm gold bead fiducials and refined to SDs below 0.8 pixels. A weighted back-projection algorithm, as implemented in the IMOD reconstruction package (Kremer et al., 1996), was used to convert the information present in the series of tilted projection images into 3D density maps (tomograms). The 3D tomographic volumes were visualized in the environment of the program Amira (TGS). Potential areas of interest were denoised using the 3D nonlinear anisotropic diffusion edge enhancing program implemented in IMOD, with 15 iterations and κ of 6.4, allowing clearer visualization.

### Subtomogram Averaging

Two chemotaxis receptor patches were selected from cryo-tomograms for subtomogram alignment and averaging. Projection series were corrected for the contrast transfer function (CTF) using TomoCTF (Fernández et al., 2006) and aligned in IMOD (Kremer et al., 1996). Tomograms were reconstructed using simultaneous iterative reconstruction technique as implemented in the IMOD reconstruction package. Subvolumes were extracted using a reference free approach, and orientations were determined using the alignment by classification strategy as implemented in Protomo/i3 software (Winkler, 2007). Data from ~400 subvolumes classified as trimer of CheA dimer/receptor complex were aligned iteratively and averaged. The density was low-pass filtered to the frequency at 0.5 Fourier shell correlation (~33 Å) and clearly shows retention of the soluble cytoplasmic protein CheA, as visualized in Chimera (Pettersen et al., 2004).

## SUPPLEMENTAL INFORMATION

Supplemental Information includes two figures and four movies and can be found with this article online at http://dx.doi.org/10.1016/j.str.2014.09.017.

## ACKNOWLEDGMENTS

The authors thank Dr. Ry Young (Texas A&M) for the ΦX174 E gene plasmid, Dr. Robert Nakamoto (University of Virginia) for the $F_0F_1$ ATP synthase antibodies, and Dr. Teresa Brosenitsch for critical reading of the manuscript. This work was supported by NIH grants GM085043 and RR024424 to P.Z. The FIB/SEM data collected at New York Structural Biology Center was made possible by a grant from New York State of Science, Technology, and Academic Research; at a facility constructed with support from the Research Facilities Improvement Program grant number C06 RR017528-01 from the National Center for Research Resources, NIH. The dual beam SEM was purchased with funds from NIH grant S10 RR029300.

Received: May 14, 2014
Revised: September 22, 2014
Accepted: September 27, 2014
Published: November 20, 2014

## REFERENCES

Al-Amoudi, A., Studer, D., and Dubochet, J. (2005). Cutting artefacts and cutting process in vitreous sections for cryo-electron microscopy. J. Struct. Biol. *150*, 109–121.

Bai, X.C., Fernandez, I.S., McMullan, G., and Scheres, S.H. (2013). Ribosome structures to near-atomic resolution from thirty thousand cryo-EM particles. eLife *2*, e00461.

Bammes, B.E., Rochat, R.H., Jakana, J., Chen, D.H., and Chiu, W. (2012). Direct electron detection yields cryo-EM reconstructions at resolutions beyond 3/4 Nyquist frequency. J. Struct. Biol. *177*, 589–601.

Barton, B., Rhinow, D., Walter, A., Schröder, R., Benner, G., Majorovits, E., Matijevic, M., Niebel, H., Müller, H., Haider, M., et al. (2011). In-focus electron microscopy of frozen-hydrated biological samples with a Boersch phase plate. Ultramicroscopy *111*, 1696–1705.

Bernhardt, T.G., Roof, W.D., and Young, R. (2000). Genetic evidence that the bacteriophage phi X174 lysis protein inhibits cell wall synthesis. Proc. Natl. Acad. Sci. USA *97*, 4297–4302.

Bernhardt, T.G., Struck, D.K., and Young, R. (2001a). The lysis protein E of phi X174 is a specific inhibitor of the MraY-catalyzed step in peptidoglycan synthesis. J. Biol. Chem. *276*, 6093–6097.

Bernhardt, T.G., Wang, I.N., Struck, D.K., and Young, R. (2001b). A protein antibiotic in the phage Qbeta virion: diversity in lysis targets. Science *292*, 2326–2329.

Bernhardt, T.G., Roof, W.D., and Young, R. (2002). The Escherichia coli FKBP-type PPIase SlyD is required for the stabilization of the E lysis protein of bacteriophage phi X174. Mol. Microbiol. *45*, 99–108.

Briegel, A., Ortega, D.R., Tocheva, E.I., Wuichet, K., Li, Z., Chen, S., Müller, A., Iancu, C.V., Murphy, G.E., Dobro, M.J., et al. (2009). Universal architecture of bacterial chemoreceptor arrays. Proc. Natl. Acad. Sci. USA *106*, 17181–17186.

Briegel, A., Li, X., Bilwes, A.M., Hughes, K.T., Jensen, G.J., and Crane, B.R. (2012). Bacterial chemoreceptor arrays are hexagonally packed trimers of receptor dimers networked by rings of kinase and coupling proteins. Proc. Natl. Acad. Sci. USA *109*, 3766–3771.

Campbell, M.G., Cheng, A., Brilot, A.F., Moeller, A., Lyumkis, D., Veesler, D., Pan, J., Harrison, S.C., Potter, C.S., Carragher, B., and Grigorieff, N. (2012). Movies of ice-embedded particles enhance resolution in electron cryo-microscopy. Structure *20*, 1823–1828.

Carlson, L.A., de Marco, A., Oberwinkler, H., Habermann, A., Briggs, J.A., Kräusslich, H.G., and Grünewald, K. (2010). Cryo electron tomography of native HIV-1 budding sites. PLoS Pathog. *6*, e1001173.

Dewey, J.S., Savva, C.G., White, R.L., Vitha, S., Holzenburg, A., and Young, R. (2010). Micron-scale holes terminate the phage infection cycle. Proc. Natl. Acad. Sci. USA *107*, 2219–2223.

Fernández, J.J., Li, S., and Crowther, R.A. (2006). CTF determination and correction in electron cryotomography. Ultramicroscopy *106*, 587–596.

Fukuda, Y., Fukazawa, Y., Danev, R., Shigemoto, R., and Nagayama, K. (2009). Tuning of the Zernike phase-plate for visualization of detailed ultrastructure in complex biological specimens. J. Struct. Biol. *168*, 476–484.

Guerrero-Ferreira, R.C., and Wright, E.R. (2014). Zernike phase contrast cryo-electron tomography of whole bacterial cells. J. Struct. Biol. *185*, 129–133.

Hayles, M.F., de Winter, D.A., Schneijdenberg, C.T., Meeldijk, J.D., Luecken, U., Persoon, H., de Water, J., de Jong, F., Humbel, B.M., and Verkleij, A.J. (2010). The making of frozen-hydrated, vitreous lamellas from cells for cryo-electron microscopy. J. Struct. Biol. *172*, 180–190.

Kaback, H.R. (1972). Transport across isolated bacterial cytoplasmic membranes. Biochim. Biophys. Acta *265*, 367–416.

Kellenberger, E., Johansen, R., Maeder, M., Bohrmann, B., Stauffer, E., and Villiger, W. (1992). Artefacts and morphological changes during chemical fixation. J. Microsc. *168*, 181–201.

Khursigara, C.M., Wu, X., and Subramaniam, S. (2008). Chemoreceptors in Caulobacter crescentus: trimers of receptor dimers in a partially ordered hexagonally packed array. J. Bacteriol. *190*, 6805–6810.

Koning, R.I., Zovko, S., Bárcena, M., Oostergetel, G.T., Koerten, H.K., Galjart, N., Koster, A.J., and Mieke Mommaas, A. (2008). Cryo electron tomography of vitrified fibroblasts: microtubule plus ends in situ. J. Struct. Biol. *161*, 459–468.

Kremer, J.R., Mastronarde, D.N., and McIntosh, J.R. (1996). Computer visualization of three-dimensional image data using IMOD. J. Struct. Biol. *116*, 71–76.

Kürner, J., Frangakis, A.S., and Baumeister, W. (2005). Cryo-electron tomography reveals the cytoskeletal structure of Spiroplasma melliferum. Science *307*, 436–438.

Leduc, M., Kasra, R., and van Heijenoort, J. (1982). Induction and control of the autolytic system of Escherichia coli. J. Bacteriol. *152*, 26–34.

Li, Z., and Jensen, G.J. (2009). Electron cryotomography: a new view into microbial ultrastructure. Curr. Opin. Microbiol. *12*, 333–340.

Li, X., Mooney, P., Zheng, S., Booth, C.R., Braunfeld, M.B., Gubbens, S., Agard, D.A., and Cheng, Y. (2013). Electron counting and beam-induced motion correction enable near-atomic-resolution single-particle cryo-EM. Nat. Methods *10*, 584–590.

Liu, J., Hu, B., Morado, D.R., Jani, S., Manson, M.D., and Margolin, W. (2012). Molecular architecture of chemoreceptor arrays revealed by cryoelectron tomography of Escherichia coli minicells. Proc. Natl. Acad. Sci. USA *109*, E1481–E1488.

Lubitz, W., Witte, A., Eko, F.O., Kamal, M., Jechlinger, W., Brand, E., Marchart, J., Haidinger, W., Huter, V., Felnerova, D., et al. (1999). Extended recombinant bacterial ghost system. J. Biotechnol. *73*, 261–273.

Maratea, D., Young, K., and Young, R. (1985). Deletion and fusion analysis of the phage phi X174 lysis gene E. Gene *40*, 39–46.

Marko, M., Hsieh, C., Schalek, R., Frank, J., and Mannella, C. (2007). Focused-ion-beam thinning of frozen-hydrated biological specimens for cryo-electron microscopy. Nat. Methods *4*, 215–217.

Medalia, O., Weber, I., Frangakis, A.S., Nicastro, D., Gerisch, G., and Baumeister, W. (2002). Macromolecular architecture in eukaryotic cells visualized by cryoelectron tomography. Science *298*, 1209–1213.

Mendel, S., Holbourn, J.M., Schouten, J.A., and Bugg, T.D. (2006). Interaction of the transmembrane domain of lysis protein E from bacteriophage phiX174 with bacterial translocase MraY and peptidyl-prolyl isomerase SlyD. Microbiology *152*, 2959–2967.

Milne, J.L., and Subramaniam, S. (2009). Cryo-electron tomography of bacteria: progress, challenges and future prospects. Nat. Rev. Microbiol. *7*, 666–675.

Murata, K., Liu, X., Danev, R., Jakana, J., Schmid, M.F., King, J., Nagayama, K., and Chiu, W. (2010). Zernike phase contrast cryo-electron microscopy and tomography for structure determination at nanometer and subnanometer resolutions. Structure *18*, 903–912.

Parkinson, J.S., and Houts, S.E. (1982). Isolation and behavior of Escherichia coli deletion mutants lacking chemotaxis functions. J. Bacteriol. *151*, 106–113.

Pettersen, E.F., Goddard, T.D., Huang, C.C., Couch, G.S., Greenblatt, D.M., Meng, E.C., and Ferrin, T.E. (2004). UCSF Chimera—a visualization system for exploratory research and analysis. J. Comput. Chem. *25*, 1605–1612.

Poole, R.K. (1993). The isolation of membranes from bacteria. Methods Mol. Biol. *19*, 109–122.

Reynolds, E.S. (1963). The use of lead citrate at high pH as an electron-opaque stain in electron microscopy. J. Cell Biol. *17*, 208–212.

Roof, W.D., Fang, H.Q., Young, K.D., Sun, J., and Young, R. (1997). Mutational analysis of slyD, an Escherichia coli gene encoding a protein of the FKBP immunophilin family. Mol. Microbiol. *25*, 1031–1046.

Studer, D., Graber, W., Al-Amoudi, A., and Eggli, P. (2001). A new approach for cryofixation by high-pressure freezing. J. Microsc. *203*, 285–294.

Szostak, M.P., Hensel, A., Eko, F.O., Klein, R., Auer, T., Mader, H., Haslberger, A., Bunka, S., Wanner, G., and Lubitz, W. (1996). Bacterial ghosts: non-living candidate vaccines. J. Biotechnol. *44*, 161–170.

Szostak, M.P., Mader, H., Truppe, M., Kamal, M., Eko, F.O., Huter, V., Marchart, J., Jechlinger, W., Haidinger, W., Brand, E., et al. (1997). Bacterial ghosts as multifunctional vaccine particles. Behring Inst. Mitt. *98*, 191–196.

Trueba, F.J., and Woldringh, C.L. (1980). Changes in cell diameter during the division cycle of Escherichia coli. J. Bacteriol. *142*, 869–878.

Wang, I.N., Smith, D.L., and Young, R. (2000). Holins: the protein clocks of bacteriophage infections. Annu. Rev. Microbiol. *54*, 799–825.

Wang, K., Strunk, K., Zhao, G., Gray, J.L., and Zhang, P. (2012). 3D structure determination of native mammalian cells using cryo-FIB and cryo-electron tomography. J. Struct. Biol. *180*, 318–326.

Winkler, H. (2007). 3D reconstruction and processing of volumetric data in cryo-electron tomography. J. Struct. Biol. *157*, 126–137.

Witte, A., and Lubitz, W. (1989). Biochemical characterization of phi X174-protein-E-mediated lysis of Escherichia coli. Eur. J. Biochem. / FEBS *180*, 393–398.

Witte, A., Bläsi, U., Halfmann, G., Szostak, M., Wanner, G., and Lubitz, W. (1990a). Phi X174 protein E-mediated lysis of Escherichia coli. Biochimie *72*, 191–200.

Witte, A., Wanner, G., Bläsi, U., Halfmann, G., Szostak, M., and Lubitz, W. (1990b). Endogenous transmembrane tunnel formation mediated by phi X174 lysis protein E. J. Bacteriol. *172*, 4109–4114.

Young, R. (1992). Bacteriophage lysis: mechanism and regulation. Microbiol. Rev. *56*, 430–481.

Young, K.D., and Young, R. (1982). Lytic action of cloned phi X174 gene E. J. Virol. *44*, 993–1002.

Zhang, P., Bos, E., Heymann, J., Gnaegi, H., Kessel, M., Peters, P.J., and Subramaniam, S. (2004). Direct visualization of receptor arrays in frozen-hydrated sections and plunge-frozen specimens of E. coli engineered to overproduce the chemotaxis receptor Tsr. J. Microsc. *216*, 76–83.

Zhang, P., Khursigara, C.M., Hartnell, L.M., and Subramaniam, S. (2007). Direct visualization of Escherichia coli chemotaxis receptor arrays using cryo-electron microscopy. Proc. Natl. Acad. Sci. USA *104*, 3777–3781.

Zheng, Y., Struck, D.K., Bernhardt, T.G., and Young, R. (2008). Genetic analysis of MraY inhibition by the phiX174 protein E. Genetics *180*, 1459–1466.

Zheng, Y., Struck, D.K., and Young, R. (2009). Purification and functional characterization of phiX174 lysis protein E. Biochemistry *48*, 4999–5006.

 